# Thermalization propagation front and robustness against avalanches in localized systems

Annarita Scocco, <sup>1</sup> Gianluca Passarelli, <sup>2</sup> Mario Collura, <sup>3,4</sup> Procolo Lucignano, <sup>2</sup> and Angelo Russomanno <sup>2</sup>

<sup>1</sup> Scuola Superiore Meridionale, Largo San Marcellino 10, I-80138 Napoli, Italy

<sup>2</sup> Dipartimento di Fisica "E. Pancini", Università di Napoli Federico II,

Complesso di Monte S. Angelo, via Cinthia, I-80126 Napoli, Italy

<sup>3</sup>SISSA, Via Bonomea 265, I-34136 Trieste, Italy <sup>4</sup>INFN, Sezione di Trieste, Via Valerio 2, 34127 Trieste, Italy

We investigate the robustness of the many-body localized (MBL) phase to the quantum-avalanche instability by studying the dynamics of a localized spin chain coupled to a  $T=\infty$  thermal bath through its leftmost site. By analyzing local magnetizations we estimate the size of the thermalized sector of the chain and find that it increases logarithmically slowly in time. This logarithmically slow propagation of the thermalization front allows us to lower bound the slowest thermalization time, and find a broad parameter range where it scales fast enough with the system size that MBL is robust against thermalization induced by avalanches. The further finding that the imbalance – a global quantity measuring localization – thermalizes over an exponential time scale both in disorder strength and system size is in agreement with these results.

#### I. INTRODUCTION

Thermalization in quantum systems occurs in a way remarkably different than in classical systems, by a mechanism called eigenstate thermalization hypothesis (ETH) [1–3]. In a thermalizing quantum system eigenstates are locally equivalent to thermal density matrices, and this gives rise to long-time thermalization of local observables [4–6]. Generic isolated quantum systems are expected to thermalize and obey ETH [7]. It is therefore of particular interest to find systems that avoid thermalization: In this case, quantum information encoded in the initial state can persist for long times, with relevance for technological applications, as quantum memories [8].

In an ergodic system, thermalization occurs because its various parts can exchange particles and energy, so a possible way for a system to avoid thermalization is to exhibit insulating behavior, an example of which is given by Anderson localization [9], occurring in noninteracting disordered systems. In the presence of small enough interactions, the system is still space localized and non thermalizing, a phenomenon called many-body localization (MBL) [10]. Following the works [11, 12], this topic has been tremendously explored over the past few years, from a theoretical [13–15], experimental [16– 21], and numerical [22–33] point of view, particularly focusing on one-dimensional systems. MBL systems display many interesting features such as the emergence of a complete set of quasi-localized integrals of motion [34–36], area law entanglement in all many-body eigenstates [25, 37, 38], logarithmic growth of entanglement entropy with time [23, 37, 39, 40]. This last slowentanglement-growth property is especially relevant, due the role played by entanglement in giving rise to ETH of local observables [41] (a thermal local density matrix is maximally mixed, and so any subsystem thermalizes becoming maximally entangled with the rest). The properties of MBL systems have been extensively described in

different reviews [42–44].

However, the stability of this phase has been put into question in the thermodynamic limit, as it was pointed out that under certain circumstances many-body localized systems may be unstable towards rare regions of small disorder by a mechanism dubbed "quantum avalanches" [45]. In different works, they have attempted to tackle the matter of one- or higher-dimensional systems both theoretically [46–49] and experimentally [50, 51], studying the spectral properties or the dynamics of a MBL system in contact with an ergodic inclusion [52–54]. In some important cases the effect of the ergodic inclusion was studied using a Lindbladian acting on an end of the system [55–57], as we better clarify below. [58]

The search for evidence of the avalanche mechanism in standard MBL models is still very active. One possible approach is through many-body resonances, which allow globally different spin configurations to interact [57, 59, 60]. They are negligible in the MBL phase but there is a crossover regime where they become more and more relevant with increasing system size, leading eventually to avalanches [57], that spread just thanks to strong many-body resonances between rare near-resonant eigenstates [61], and are related to interaction-driven instabilities seen in the behavior of correlation lengths [62]. Avalanches are also investigated from the experimental point of view, as in Ref. [50], where they monitor avalanche spread by measuring the site-resolved entropy over time.

The approach we are interested in is based on the idea that an ergodic inclusion, which occurs almost certainly in sufficiently large systems, can thermalize the entire chain if the thermalization time of any subchain is short enough [57]. This time can be numerically estimated by coupling a subchain to a thermal bath by one of its ends, simulating the already thermalized part of the chain. If the slowest thermalization time, corresponding to the time it takes for the farthest spin to thermalize, scales slowly enough with the size of the subchain, then the

avalanche propagates and the system thermalizes [55, 57].

In this work, we adopt a similar approach by coupling an MBL system to a  $T = \infty$  thermal bath by one of its extremities and study how the slowest thermalization time scales with the system size, to understand if MBL is robust to avalanches. We use the Lindbladian bath considered in Ref. [63] restricting it to just the leftmost site of the system. [55–57] This choice of bath can be easily studied with an approach of Hamiltonian quantum trajectories and can provide a lower bound to the slowest thermalization time. Furthermore, it allows scaling to large system sizes in the case of Anderson localized systems, which also provide useful information for the MBL case, as the coupling to the bath makes the system interacting [52]. Although the chain coupled to the bath is not integrable, one can show that the dynamics is equivalent to an average over many realizations, which we refer to as quantum trajectories, of a unitary Schrödinger evolution with noisy Hamiltonian (unitary unraveling [64]). Along each stochastic trajectory, the system is integrable and can be described by a Gaussian state, enabling in the Anderson localized case a numerical analysis up to larger system sizes.

We focus on scaling the slowest thermalization time with the system size by looking at the propagation of the thermalization front through the chain, an approach that, to the best of our knowledge, has not yet been used in this context. Heat propagates through the system, from the bath at the leftmost site, and at any time there is a subchain on the left side that has already thermalized [see the cartoon in Fig. 1]. We estimate the length of this thermalized subchain by defining a thermalization length scale based on the behavior of the local magnetizations. We find that both in Anderson and MBL localized systems this length scale increases logarithmically in time, and use this logarithmic growth to estimate the time in which the thermalization front reaches the other end of the chain. We find that this time scale exponentially increases with the system size, and there is a regime of parameters where this exponential increase is fast enough that localization is robust against thermalization induced by avalanches. We also study the slowest thermalization time by looking at the thermalization behavior of the imbalance and obtain results in agreement.

The paper is organized as follows. In Sec. II we define our model, and in Sec. III we discuss the numerical methods we use in the case of many-body localization. In Sec. IV A we numerically show that the imbalance thermalization time is exponential both in the system size and in the disorder strength, and this allows us to show that there is a critical strength beyond which MBL is robust against the avalanche instability. In Sec. IV B we define a thermalization length scale using the local magnetizations and show that it logarithmically increases with time. This implies that the thermalization time of the imbalance exponentially increases with system size. In Sec. V we draw our conclusions and sketch perspectives of future work. In the Appendixes we discuss some

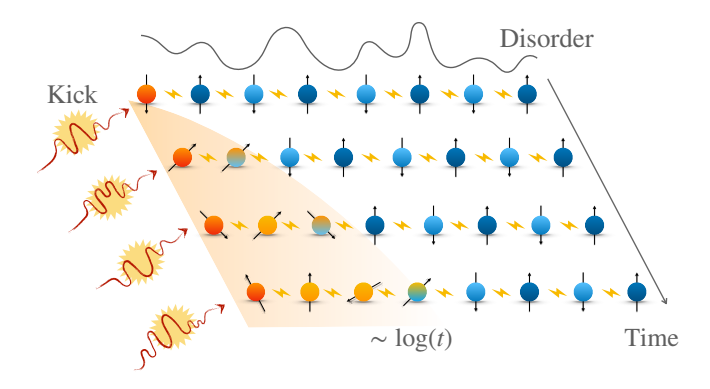


FIG. 1. Graphical visualization of the model: a 1D chain of interacting 1/2 spins with a fixed disorder profile, starting from the Néel state, and with open boundary conditions. Different copies of the system mean different subsequent times, as indicated by the time arrow on the right. The leftmost spin is coupled to a  $T=\infty$  thermal bath (a time-dependent kick) and a thermalization front (shaded area) propagates logarithmically slowly.

important aspects that would have broken the main discussion. In particular, in Appendix A we review how the Hamiltonian quantum-trajectory approach works, in Appendix B we discuss how the Gaussian nature of the state in the case of the Anderson model simplifies the numerical analysis, and in Appendix C we review the derivation of the threshold above which the scaling of the slowest thermalization time is slow enough to guarantee robustness against avalanches.

#### II. MODEL

We consider the 1D spin-1/2 XXZ Heisenberg model in a random magnetic field

$$\hat{H}_0 = \sum_{j=1}^{L} h_j \hat{S}_j^z + J \sum_{j=1}^{L-1} (\hat{S}_j^x \hat{S}_{j+1}^x + \hat{S}_j^y \hat{S}_{j+1}^y + \Delta \hat{S}_j^z \hat{S}_{j+1}^z),$$
(1)

where L is the system size,  $\hat{S}_j^{\alpha} \equiv \hat{\sigma}_j^{\alpha}/2$  are the on-site magnetizations ( $\alpha \in \{x,y,z\}$ ) and J=1 sets the energy scale. The on-site magnetic field  $h_j$  are chosen randomly and uniformly in the interval [-W,W], and the system conserves the total magnetization  $S_{\text{tot}}^z = \sum_{j=1}^L \hat{S}_j^z$  in the z-direction. We consider open boundary conditions.

This model was widely studied as a paradigmatic model displaying MBL behavior [23, 28, 65–70] for several reasons. It exhibits a transition from the ergodic to the MBL phase at a critical disorder strength  $W_c$ , and it is believed to capture all essential properties of the MBL phase and of the localization transition. At  $\Delta=1$  various estimates of  $W_c$  have been made collocating  $3.5 \lesssim W_c \lesssim 5.4$  [22, 24, 28, 62, 71, 72], although the debate is still open. Furthermore, the Jordan-Wigner transformation [73] allows to map this model to a system

of interacting spinless fermions with tunneling matrix element J and nearest-neighbor interaction strength  $\Delta$  (see Appendix B for details), connecting the model and the experiments on quasirandom optical lattices [16].

We couple one end of this system to a thermal bath that induces  $T=\infty$  thermalization. This evolution is described by the Lindbladian

$$\dot{\hat{\rho}}(t) = -i[\hat{H}_0, \hat{\rho}(t)] - \gamma^2[\hat{S}_1^z, [\hat{S}_1^z, \hat{\rho}(t)]], \qquad (2)$$

where  $\gamma^2$  is the coupling to the bath. Restricting to any  $S_{\text{tot}}^z$  subspace, one can see that the identity is the only steady state of this Lindblad dynamics, implying the  $T = \infty$  thermalization inside that subspace. A similar Lindbladian, acting on all the sites and not just on the first one, has been studied in [63].

In order to study this Lindbladian, we use a quantum trajectory approach. More specifically we rely on the so-called unitary unraveling [64] where the dynamics of Eq. (2) is described by an average over many realizations of unitary Schrödinger evolutions with a noisy Hamiltonian. So one should evolve with the kicked Hamiltonian

$$\hat{H}_{\gamma}(t) = \hat{H}_0 + \gamma \xi(t) \hat{S}_1^z, \qquad (3)$$

where  $\hat{H}_0$  is defined in Eq. (1) and  $\xi(t)$  is an uncorrelated Gaussian noise, for which  $\langle \xi(t) \rangle = 0$ ,  $\langle \xi(t)\xi(t') \rangle = \delta(t-t')$  and all the cumulants are vanishing (angular brakets denote the average over noise realizations). In order to implement it numerically, we must discretize it over time intervals  $\tau \ll 1/J$  and Trotterize it, so that the *n*-th evolution step is given by the action of the operator

$$\hat{U}_n = e^{-i\eta_n \gamma \hat{S}_1^z} e^{-i\tau \hat{H}_0} , \qquad (4)$$

where  $\eta_n$  are Gaussian random variables such that  $\eta_n = \int_{(n-1)\tau}^{n\tau} \xi(t) dt$ , so that  $\langle \eta_n \rangle = 0$  and  $\langle \eta_n \eta_{n'} \rangle = \tau \delta_{n,n'}$ . In the following we fix  $\tau = 0.05$  (choosing a shorter  $\tau$  does not affect the results). Averaging over random realizations, in the limit  $\tau \to 0$  one recovers the Lindblad equation, Eq. (2), as we show in Appendix A, and in the Anderson-model case  $\Delta = 0$  the dynamics along each trajectory is given by Gaussian states, allowing thereby to numerically address large system sizes , as we discuss in detail in Appendix B.

### III. METHODS

For the dynamics, it is customary to evolve the system starting from the high energy, out-of-equilibrium, unentangled, antiferromagnetic Néel state  $|\psi\rangle = |\uparrow\downarrow\dots\uparrow\downarrow\rangle$ , which has total magnetization  $S_{\text{tot}}^z=0$  and is included in the smaller sector of the Hilbert space of dimension  $\mathcal{N}=\binom{L}{L/2}$ . In order to detect the effect of the kick on the localized chain, we compare two different evolutions, one with the Hamiltonian, Eq. (1), without noise  $(\gamma=0)$ 

$$|\psi_0(t)\rangle = e^{-i\hat{H}_0 t} |\uparrow\downarrow\uparrow\downarrow...\rangle ,$$
 (5)

and one with the fully noisy Hamiltonian  $\hat{H}_{\gamma}$  [Eq. (3)], fixing the same disorder realization

$$|\psi_{\gamma}(t)\rangle = \prod_{n=1}^{[t/\tau]} \hat{U}_n |\uparrow\downarrow\uparrow\downarrow...\rangle ,$$
 (6)

ending both evolutions at some final time  $t_f$ . The state  $|\psi_0(t)\rangle$  is unaffected by noise and will be considered as a reference. We average each of the quantities over  $N_r$  different disorder/noise realizations. When  $\gamma=0$  in each realization we take a different random choice of the onsite fields  $h_j$ , for  $j\in\{1,\ldots,L\}$  in Eq. (1). When  $\gamma=1$  we take in each realization a different choice of the  $h_j$  and also a different choice of the random sequence  $\eta_n$ , with  $n\in\{1,\ldots,[t_f/\tau]\}$  providing the noise in Eq. (4). We indicate the average over the  $N_r$  disorder/noise realizations with an overline  $\overline{(\ldots)}$ . We evaluate the errorbar on this average as the root mean square deviation divided by  $\sqrt{N_r}$ , performing error propagation where appropriate.

In the case of the Anderson model we take  $N_r=1200$  while in the case of MBL, in which the simulation times are longer, the number of realizations will be going from  $N_r=500$  for the smallest system L=8, to  $N_r=100$  for the biggest one L=16. When we compare  $\gamma=1$  and  $\gamma=0$  we average over the same set of disorder realization. To simulate the time evolution we use exact diagonalization and Krylov subspace projection methods [74]. Exact diagonalization is much more efficient in the case of the Anderson model ( $\Delta=0$ ) thanks to the mapping of each trajectory to a free fermion model (see Sec. B). In the following text, whenever we consider an interacting case, we fix  $\Delta=1$ , and when we consider coupling to the thermal bath we take  $\gamma=1$ .

## IV. IMBALANCE AND LOCAL MAGNETIZATIONS

# A. Imbalance behavior and robustness against avalanche instability

The imbalance  $\mathcal I$  between the even and odd sites in the spin representation is defined as

$$\mathcal{I}(t) = \frac{1}{L} \sum_{i=1}^{L} (-1)^j \langle \psi(t) | \hat{S}_j^z | \psi(t) \rangle. \tag{7}$$

It is a global feature of the system which can be computed from local quantities, and can be experimentally measured [16, 75]. The normalization ensures  $\mathcal{I}(t=0)=1$ . The long-time stationary value of the imbalance effectively serves as an order parameter of the MBL phase, which is why it has been widely used in the literature [65, 72, 76]. For disorder strength  $W < W_c$ , a power-law decay  $\mathcal{I}(t) \propto t^{-\beta}$  has been observed [76], while, in localized ones for  $W > W_c$ , one numerically sees convergence to a constant value at long times [44], indicating

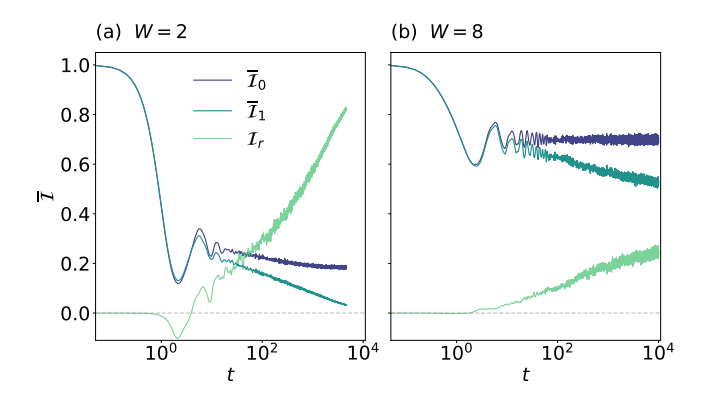


FIG. 2. Interacting case. Time evolution of the imbalance in the unkicked case  $\overline{\mathcal{I}}_0$ , in the kicked case  $\overline{\mathcal{I}}_1$  and relative difference  $\mathcal{I}_r$  for L=16, for W=2 in panel (a) and W=8 in panel (b), and  $N_r=100$ .

the existence of a set of conserved quantities preserving local information about its initial state. (See [65] for the challenges related to numerically observing the latter regime.)

The goal of our analysis is to understand how the imbalance applying the kick  $\overline{\mathcal{I}}_{\gamma=1}$  differs from the unbiased case,  $\overline{\mathcal{I}}_{\gamma=0}$ , scaling the size of the system L and the strength of the disorder W. We show some examples of the behavior of the imbalance in Fig. 2 for L=16 and two different values of W [W=2 in panel (a) and W=8 in panel (b)]. We see that the coupling to the bath  $\gamma$  causes  $\overline{\mathcal{I}}_{\gamma}(t)$  to deviate from  $\overline{\mathcal{I}}_{0}(t)$  starting at a time  $t\sim 1$ , eventually decaying to zero.

In order to perform a size scaling we define a relative imbalance  $\mathcal{I}_r$  as

$$\mathcal{I}_r(t) = \frac{\overline{I}_0(t) - \overline{I}_{\gamma}(t)}{\overline{I}_0(t)}.$$
 (8)

This quantity increases from the initial value  $\mathcal{I}_r(t=0)=0$  [due to  $\overline{\mathcal{I}}_0(t=0)=\overline{\mathcal{I}}_\gamma(t=0)$ ] to the asymptotic value  $\mathcal{I}_r(t\to\infty)=1$  [due to  $\overline{\mathcal{I}}_\gamma(t\to\infty)=0$ ], as we see in Fig. 2. We can study the time scale over which this happens and we do that computing the minimum time  $\widetilde{t}$  it takes for the relative imbalance  $\mathcal{I}_r$  to grow above a fixed threshold, within the statistical error. Given the computational limitations, we fixed the common threshold to be  $r_{\rm th}=0.17$ . [77]

We show results in Fig. 3. From one side we see that  $\tilde{t}$  displays a behavior consistent with an exponential increase with the disorder strength W, as the fits in Fig. 3(a) shows. This is in agreement with the exponential dependence on the disorder strength of the thermalization time, seen when one end of a MBL chain is time-periodically coupled to an ergodic one [54]. From the other side we find that  $\tilde{t}$  also exponentially increases with the size L of the system, as we show in Fig. 3(b).

So we conclude that, at least for the parameters considered in Fig. 3, there is some  $\alpha > 0$  such that the

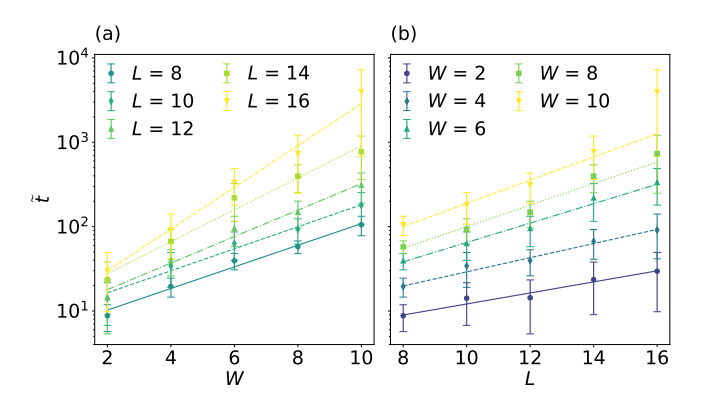


FIG. 3. Interacting case. (Panel a)  $\widetilde{t}$  versus W for different values of L. (Panel b)  $\widetilde{t}$  as a function of L for different values of W. The error bars are the maximum error,  $N_r$  goes from 500 for L=8 to 100 for L=16.

thermalization time of the imbalance has the behavior

$$\tilde{t} \sim \exp(\alpha LW)$$
. (9)

We use the argument of Ref. [57], according to which MBL is robust if the slowest thermalization time  $t_s$  grows faster than  $4^L$  (see Appendix C for more details), and the fact that  $\tilde{t}$  is a lower bound to  $t_s$ , as by definition  $t_s > \tilde{t}$ , to find that there is a minimum value of disorder

$$\widetilde{W} = \frac{2\ln 2}{\alpha} \tag{10}$$

such that for  $W > \widetilde{W}$  MBL is robust against avalanche instability. We underline that MBL could still be robust even for  $W < \widetilde{W}$ , because  $t_s$  might still grow faster than  $4^L$ . If the scaling behavior observed in Fig. 3 holds over a sufficiently wide range of parameters, there exists a disorder strength beyond which MBL remains robust.

To gain a deeper understanding of the imbalance behavior, we will focus on the properties of the local magnetizations in the next section.

#### B. Thermalization front and local magnetizations

In order to better understand the behavior of the imbalance, let us consider the local magnetizations  $\overline{(S_j^z)}_{\gamma}(t) = \overline{\langle \psi_t | \hat{S}_j^z | \psi_t \rangle}$  for the evolution with a given  $\gamma$ . To see how thermalization propagates through the chain, let us set

$$\delta S_j(t) = \left| \overline{(S_j^z)}_{\gamma=0}(t) - \overline{(S_j^z)}_{\gamma=1}(t) \right| , \qquad (11)$$

and define a thermalization length scale as

$$h(t) = \frac{\sum_{j=1}^{L} (j-1)\delta S_j(t)}{\sum_{j=1}^{L} \delta S_j(t)},$$
(12)

and study its behavior as a function of time. We plot h(t)versus t for the Anderson-model case in Fig. 4(a) and in the interacting case in Fig. 4(b). In the Anderson-model case, whatever the disorder strength W, we see that h(t)logarithmically increases with time for t large enough, as  $h(t) \sim A \ln(t)$ . The same occurs in the interacting case, when  $W > W_c$  and one is inside the MBL regime. We also show the behavior for W=2, in which we can see that h(t) is starting to saturate to a constant value. To track how fast this length grows we can obtain the slope A with a linear fit of h(t) as a function of  $\ln t$ , applying the fit for times such that the linear regime in ln t has already set in, showing the linear fit in blue. We plot the 1/A resulting from this fit as a function of W in the insets of Fig. 4. In the Anderson-model case we see that 1/Airregularly increases with W, while in the interacting case the increase is more regular, slightly faster than linear.

So we have found that the thermalization front propagates logarithmically, giving rise to some interesting predictions on the behavior of  $\mathcal{I}_r(t)$ . Because at time t only a fraction  $f(t) \sim A \ln(t)/L$  of the chain has thermalized, we can predict a behavior

$$\mathcal{I}_r(t) \sim A \ln(t) / L$$
. (13)

We have obtained this estimate as follows. Due to extensivity, let us write the long-time value of the noiseless imbalance  $\bar{I}_0(t)=qL$  for some  $q\in(0,1)$  and  $t\gg 1/J$ . If only a fraction of f(t) sites has thermalized, we can roughly approximate  $\bar{I}_\gamma(t)\sim Lq[1-f(t)]$ , and so we apply Eq. (8) and get Eq. (13), valid for  $t\gg 1/J$ .

We have numerically checked that this prediction is obeyed for large L in the Anderson case as we show in Fig. 5(a), and for smaller system sizes in the interacting case as we show in Fig. 5(b). In both panels we fix W and plot  $L\mathcal{I}_r(t)$  versus t for different values of L, with a logarithmic scale on the horizontal axis. We see that the rescaled curves tend to a limit curve, meaning that the scaling with 1/L holds for large system sizes. Furthermore, the limit curve increases linearly with time in logarithmic scale, consistently with Eq. (13). This finding implies an exponential scaling with the system size of the thermalization time of the imbalance, as the one shown in Fig. 3(b).

As we can see in the inset of Fig. 4(b), the behavior of 1/A is consistent with a linear increase in W, so we can write  $1/A \sim \beta W$  for some  $\beta > 0$ . Substituting  $1/A = \beta W$  in Eq. (13) and imposing  $\mathcal{I}_r(\tilde{t}) = r_{\rm th} (= 0.17)$  we get

$$\widetilde{t} \sim \exp\left(r_{\rm th}\beta LW\right)$$
,

that is consistent with Eq. (9).

Let us see what the results above imply for robustness of localization against avalanches. In Sec. IV we have derived the threshold value in Eq. (10), which implies the robustness of MBL for W large enough. Let us now assume to average over infinite disorder/randomness realization and observe that Eq. (11) implies

$$\delta S_j(\infty) = \lim_{t \to \infty} \delta S_j(t) = \lim_{t \to \infty} \left| \overline{(S_j^z)}_{\gamma=0}(t) \right| , \qquad (14)$$

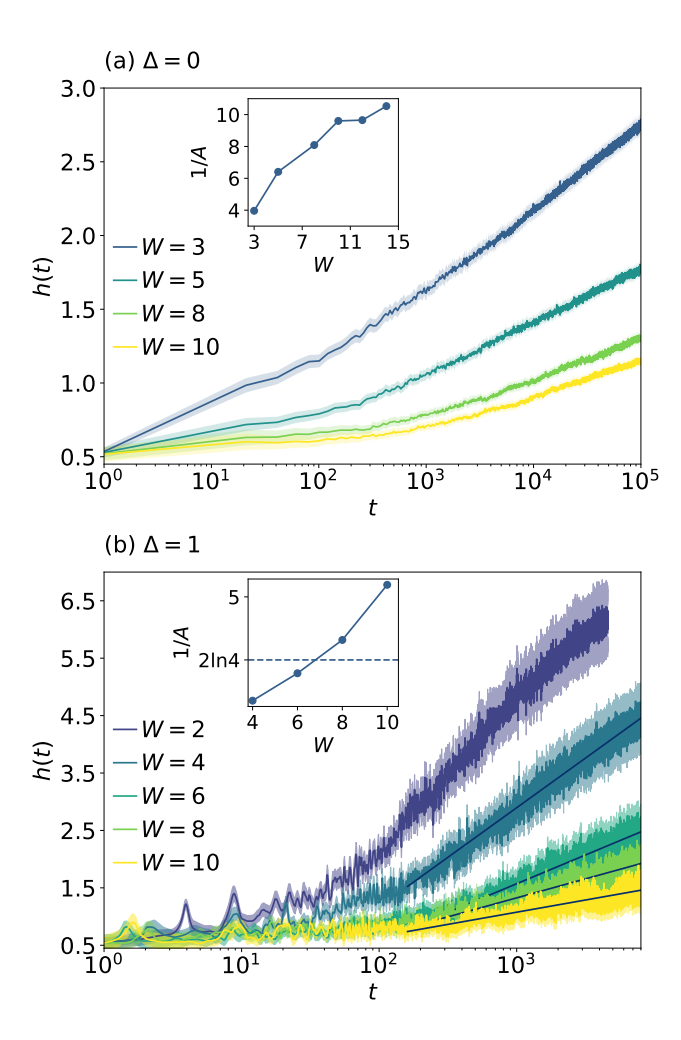


FIG. 4. (Main panels) h(t) versus t in the Anderson ( $\Delta=0$ ) case in panel (a) and interacting case ( $\Delta=1$ ) in panel (b). Notice the logarithmic scale on the horizontal axis. (Insets) 1/A versus W, where A is the slope obtained linearly fitting h(t) versus  $\ln t$ , applying the fit for times large enough that the linear in  $\ln t$  regime has already set in. In the inset in panel (b) there is the reference value  $1/A=4\ln 2$  as defined in Eq. (18). Numerical parameters in (a):  $L=100, N_r=1200$ . Numerical parameters in (b):  $L=16, N_r=100$ .

because  $\lim_{t\to\infty} \overline{(S_j^z)}_{\gamma=1}(t) = 0 \ \forall j=1,\ldots,L$  due to thermalization. In periodic boundary conditions (PBC), due to the symmetries of the problem averaged over disorder, both  $\left|\overline{(S_j^z)}_{\gamma=0}(t)\right|$  and  $\delta S_j(\infty)$  are independent of j, (let us write  $\delta S_j(\infty) \equiv \delta S$ ), so that

$$\lim_{t \to \infty} h(t) = \frac{\delta S \sum_{j=1}^{L} (j-1)}{\delta S \sum_{j=1}^{L} 1} = \frac{L-1}{2} \quad \text{ for PBC}. (15)$$

The open boundary conditions affect the behavior of the  $\left|\overline{(S_j^z)}_{\gamma=0}(t)\right|$ , and then of the  $\delta S_j(\infty)$ , for a finite length  $l_b$  near the boundaries. This length  $l_b$  is finite and does not scale with L because we assume the system with  $\gamma=0$  to be localized (Anderson or MBL). So we

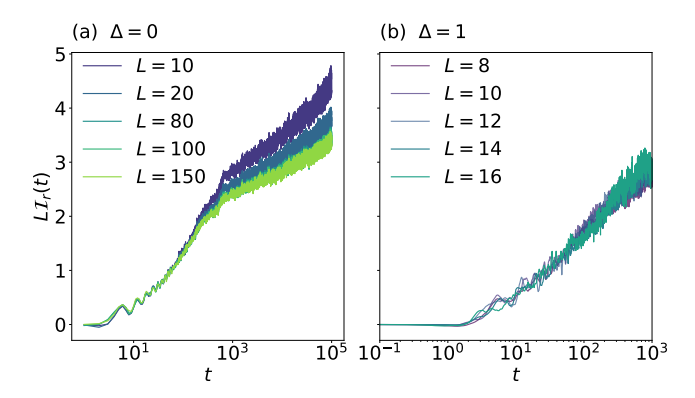


FIG. 5.  $L\mathcal{I}_r(t)$  versus t for and W=8 in the Anderson  $(\Delta=0)$  case in panel (a) and in the interacting case in panel (b). Notice the logarithmic scale on the horizontal axis.

can write in our case

$$\lim_{t \to \infty} h(t) = \frac{L-1}{2} + \mathcal{O}(l_b) \quad \text{for OBC}.$$
 (16)

We can say that all local magnetizations have thermalized, at time  $t^*$ , when  $h(t^*) = \lim_{t\to\infty} h(t)$ . Using that for  $t \gg 1/J$  the length scale  $h(t) \sim A \ln(t)$ , we get with some simple algebra the thermalization time  $t^*$  as

$$t^* \sim \exp\left(\frac{L}{2A}\right)$$
, (17)

with some multiplicative constants in front that are irrelevant for the scaling with L. In order to have robustness against avalanches, we must have a scaling faster than  $4^L$ . We meet this condition if  $\exp\left(\frac{1}{2A}\right) > 4$  or

$$\frac{1}{A} > 2 \ln 4$$
. (18)

In the inset of Fig. 4(a), we observe that the Anderson model consistently satisfies this requirement within the parameter range we investigate. The Anderson model is inherently integrable and unable to generate ergodic inclusions. However, if an ergodic inclusion is introduced into the model, it remains resistant to thermalization induced by avalanches within this parameter range.

In contrast, the MBL model satisfies Eq. (18) provided that W exceeds a threshold value  $W^* \gtrsim 7$ , as shown in the inset of Fig. 4(b). For  $W > W^*$ , MBL remains robust. For  $W < W^*$ , we cannot make definitive claims about stability because  $t^*$  in Eq. (17) only offers a lower bound on the slowest thermalization time  $t_s$ .

#### V. CONCLUSION AND PERSPECTIVES

In conclusion we have studied a many-body or Anderson localized model coupled to a  $T = \infty$  thermal bath by one end. The coupling is described by a Lindbladian,

and to numerically study it we have used a quantum-trajectory approach. More specifically, we have used a unitary unraveling such that the dynamics is an average over many realizations of a unitary Schrödinger evolution with noise. In the case of Anderson localization this approach allows to reach quite large system sizes, due to the Gaussian form of the state along each quantum trajectory.

We have first numerically studied the dynamics of the imbalance, a global quantity widely used to assess the presence of localization. We have defined its thermalization time as the time beyond which the normalized difference of the imbalance with and without thermal bath goes beyond a given threshold, and we see that in the MBL case this thermalization time exponentially increases with the strength of the disorder and the size of the system. We have shown that this result implies that the MBL is robust against the avalanche instability when the disorder strength goes beyond a given threshold.

We have then focused on the heat propagation through the system considering how a thermalization front propagated. We have estimated the extension of the already thermalized part of the chain, defining a thermalization length scale using the onsite magnetizations, and found that it logarithmically increases with time. This is true both for the Anderson and the MBL case and we could use it to lower bound the slowest thermalization time with a quantity exponentially scaling with the system size. We have found that in the strong-disorder regime this scaling is fast enough that the system is robust to avalanches. The thermalization front propagating logarithmically slowly suggests that the localized integrals of motion might play a role also in case of coupling to a bath, and slow down the heat propagation well below the ballistic trend predicted by the Lieb-Robinson bound [73]. The reason for this idea is that the localized integrals of motion play a strictly similar role in slowingdown the propagation of quantum correlations in an isolated MBL system, leading to a logarithmic increase of entanglement entropy. More studies are needed to clarify this point.

The perspectives of future work are exciting. First of all we can focus our attention to the density-density correlator [84], a quantity whose propagation properties are known in MBL systems, and see how its behavior is changed by the presence of a propagating thermalization front. Second, we can perform a similar analysis on the OTOC (that for MBL systems has been considered in [85]) to see how the thermalization front affects the scrambling properties of the system. Finally, we can study more deeply the relation between the strength of localization of the integrals of motion, the logarithmic thermalization front, the scaling of the slowest thermalization time, and the robustness of MBL to avalanches.

#### ACKNOWLEDGMENTS

G.P., P.L. and A.R. acknowledge financial support from PNRR MUR Project PE0000023- NQSTI and computational resources from MUR, PON "Ricerca e Innovazione 2014-2020", under Grant No. PIR01\_00011 - (I.Bi.S.Co.). G.P. acknowledges computational resources from the CINECA award under the ISCRA initiative. This work was supported by PNRR MUR project PE0000023 - NQSTI, by the European Union's Horizon 2020 research and innovation programme under Grant Agreement No 101017733, by the MUR project CN\_00000013-ICSC (P.L.), and by the QuantERA II Programme STAQS project that has received funding from the European Union's Horizon 2020 research and innovation program.

## Appendix A: Derivation of the Lindblad equation form the quantum-trajectory scheme

Let us start with the Schrödinger equation with the Hamiltonian Eq. (3)

$$i\frac{d}{dt}|\psi(t)\rangle = [\hat{H}_0 + \gamma\xi(t)\hat{S}_1^z]|\psi(t)\rangle$$
 (A1)

We can write it as

$$|\psi(t + \Delta t)\rangle \langle \psi(t + \Delta t)| = |\psi(t)\rangle \langle \psi(t)|$$

$$-i\Delta t[\hat{H}_0, |\psi(t)\rangle \langle \psi(t)|] - i\Delta W_t \gamma[\hat{S}_1^z, |\psi(t)\rangle \langle \psi(t)|],$$
(A2)

where  $\langle \Delta W_t \rangle = \Delta t$  and  $\langle \Delta W_t \Delta W_{t'} \rangle = \delta_{t,t'} \Delta t$  are Gaussian uncorrelated variables. Let us also write

$$|\psi(t)\rangle \langle \psi(t)| = |\psi(t - \Delta t)\rangle \langle \psi(t - \Delta t)|$$

$$-i\Delta t[\hat{H}_0, |\psi(t - \Delta t)\rangle \langle \psi(t - \Delta t)|] - i\Delta W_t \gamma[\hat{\sigma}_1^z, |\psi(t - \Delta t)\rangle \langle \psi(t - \Delta t)|],$$
(A3)

and substitute it in the last term of Eq. (A2). We get many terms. Averaging over randomness and defining  $\hat{\rho}_t = \langle \varrho(t) \rangle$  with  $\varrho(t) \equiv |\psi(t)\rangle \langle \psi(t)|$ , we get

$$\hat{\rho}_{t+\Delta t} = \hat{\rho}_t - i\Delta t[\hat{H}_0, \hat{\rho}_t] - (\overline{\Delta W_t \Delta W_t}) \gamma^2 [\hat{S}_1^z, [\hat{S}_1^z, \hat{\rho}_{t-\Delta t}]] + o(\Delta t).$$
(A4)

Using  $\langle \Delta W_t \Delta W_t \rangle = \Delta t$  and going in the limit  $\Delta t \to 0$  we get

$$\frac{d}{dt}\hat{\rho}_t = -i[\hat{H}_0, \hat{\rho}_t] - \gamma^2[\hat{S}_1^z, [\hat{S}_1^z, \hat{\rho}_t]]. \tag{A5}$$

#### Appendix B: Case of the Anderson model

Applying the Jordan-Wigner transformation, the model in Eq. (1) becomes the spinless-fermion model

$$\hat{H}_0 = \sum_{j=1}^{L} h_j \hat{n}_j + J \sum_{j=1}^{L-1} \left[ \frac{1}{2} (\hat{c}_j^{\dagger} \hat{c}_{j+1} + \text{H. c.}) + \Delta \hat{n}_j \hat{n}_{j+1} \right]$$
(B1)

where  $\hat{c}_j^{(\dagger)}$  are anticommuting fermionic operators acting on the j-th site. The number of fermions  $N \equiv \sum_{j=1}^L \hat{n}_j$  is conserved. In the Anderson-model case we have  $\Delta = 0$  and we get a quadratic fermionic Hamiltonian, so that the time evolved state  $|\psi(t)\rangle$  along each trajectory can be cast in the form of a generic Gaussian state (Slater determinant). The full information of such state is contained in a  $L \times N$  matrix W(t), defined by

$$|\psi(t)\rangle = \prod_{k=1}^{N} \left[ \sum_{j=1}^{L} \left[ W(t) \right]_{j,k} \hat{c}_{j}^{\dagger} \right] |\Omega\rangle , \quad (B2)$$

where  $|\Omega\rangle$  is the vacuum of the fermionic operators  $\hat{c}_j$ . Because the number of fermions is conserved and we initialize with the Néel state we have N=L/2. At initial time, the matrix  $L\times N$  matrix defining the Néel state is given by  $[W(0)]_{k,l} = \sum_{j=1}^{L/2} \delta_{2j,l}\delta_{j,k}$ . The discrete evolution step (see Eq. (4))

$$|\psi(t+\tau)\rangle = e^{-i\eta_n \gamma \hat{S}_1^z} e^{-i\tau \hat{H}_0} |\psi(t)\rangle$$
 (B3)

is simply translated in the dynamics of the matrix  $\boldsymbol{W}(t)$  as

$$W(t+\tau) = K_n e^{-i\tau Q} W(t), \qquad (B4)$$

where the noisy step is implemented through the  $L \times L$  diagonal matrix  $K_n$  with matrix element  $[K_n]_{i,j} = \delta_{i,j} + \delta_{1,i}\delta_{1,j}(e^{-i\eta_n\gamma}-1)$ , while the  $L \times L$  matrix Q implementing the action of the Anderson Hamiltonian has matrix elements  $[Q]_{i,j} = \delta_{i,j}h_j + \frac{J}{2}(\delta_{i,j+1} + \delta_{i,j-1})$ . Thanks to the validity of Wick's theorem, one can use the matrix W(t) to obtain the expectation of any observable, and even the entanglement entropy, as clarified in [64]. In this way one can numerically reach quite large system sizes, up to  $L \sim \mathcal{O}(10^2)$ .

### Appendix C: Scaling of the slowest thermalization time and robustness of localization against avalanches

In this section we explain why, in order for localization to be robust against avalanches, the slowest thermalization time should scale faster than  $4^L$  when one end of the system is coupled to a thermal bath. The thing has already been clearly explained in [55, 57], and we add this section just for completeness. Let us consider Fig. 6 depicting an MBL chain. We have an ergodic inclusion of size  $r_0$  (red region), and a part that has already thermalize (yellow region) made by two sectors, with the same size r (we assume the avalanches to act symmetrically). The rest of the system is already localized (blue region) and we want to see if thermalization can further propagate there by avalanches.

With this aim, we focus on a part of the localized region in contact with the ergodic region, made by two



FIG. 6. Scheme of an MBL chain for the analysis of robustness of MBL to avalanches. The red region is the ergodic inclusion, the yellow region the thermalized part of the chain, the blue region the part of the chain not yet thermalized. We focus on a subset of the latter (dark blue) that is in contact with the thermalized region and is made by two sectors, each of length  $\Delta r$ .

sectors of length  $\Delta r$  (dark blue region). We ask ourselves if this region thermalizes due to the contact with the yellow region, that's to say if the avalanche propagates. This can happen if each sector in the dark-blue region (let's say the right one – they are equal) thermalizes fast enough. So the slowest thermalization time  $t_s$  of each dark-blue sector must be much shorter than the inverse gap  $1/\delta$  of the region obtained joining the red, the yellow and the dark blue regions. The point is that thermalization in each dark-blue sector must be faster

than the time needed to the part of the chain involved in the thermalizing dynamics (red+yellow+dark-blue) to express finite-size revivals and other quantum dynamical effects connected with the discreteness of the spectrum that hinder thermalization. On general grounds [55, 57] (and we numerically verify it also in our work) one has  $t_s \sim \kappa^{\Delta r}$  for some  $\kappa > 0$ . Being this a spin 1/2 system one has  $\delta = 2^{-(r_0+2r+2\Delta r)}$ . Imposing  $t_s \ll 1/\delta$ , and asking that this condition should be verified also in the limit of  $\Delta r \gg r$ , one finds

$$\kappa < 4$$
. (C1)

By contrast, if  $\kappa > 4$  MBL is robust to avalanches. So it is very important to know  $\kappa$ . In order to find it, we have done as biologists do when move a portion of neural tissue from in vivo to in vitro [55, 57]: We have cut away the right blue region from the system in Fig. 6, we have connected its left site to a thermal bath simulating the yellow thermalized region in Fig. 6, and we have studied the scaling of the slowest thermalization time with  $\Delta r$ . (We have renamed  $\Delta r$  as L for merely aesthetic reasons.)

- [1] J. M. Deutsch, Phys. Rev. A 43, 2046 (1991).
- [2] M. Srednicki, Phys. Rev. E **50**, 888 (1994).
- [3] T. c. v. Prosen, Phys. Rev. E **60**, 3949 (1999).
- [4] A. Polkovnikov, K. Sengupta, A. Silva, and M. Vengalattore, Rev. Mod. Phys. 83, 863 (2011).
- [5] A. P. Luca D'Alessio, Yariv Kafri and M. Rigol, Advances in Physics 65, 239 (2016).
- [6] M. Rigol, V. Dunjko, and M. Olshanii, Nature 452, 854 (2008).
- [7] P. Reimann, Nature Communications **7**, 10.1038/ncomms10821 (2016).
- [8] M. Serbyn, M. Knap, S. Gopalakrishnan, Z. Papić, N. Y. Yao, C. R. Laumann, D. A. Abanin, M. D. Lukin, and E. A. Demler, Phys. Rev. Lett. 113, 147204 (2014).
- [9] P. W. Anderson, Phys. Rev. **109**, 1492 (1958).
- [10] L. Fleishman and P. W. Anderson, Phys. Rev. B 21, 2366 (1980).
- [11] D. Basko, I. Aleiner, and B. Altshuler, Annals of Physics 321, 1126 (2006).
- [12] I. V. Gornyi, A. D. Mirlin, and D. G. Polyakov, Phys. Rev. Lett. 95, 206603 (2005).
- [13] R. Vosk and E. Altman, Phys. Rev. Lett. **110**, 067204 (2013).
- [14] R. Vosk, D. A. Huse, and E. Altman, Phys. Rev. X 5, 031032 (2015).
- [15] J. Z. Imbrie, Journal of Statistical Physics 163, 998 (2016).
- [16] M. Schreiber, S. S. Hodgman, P. Bordia, H. P. Lüschen, M. H. Fischer, R. Vosk, E. Altman, U. Schneider, and I. Bloch, Science 349, 842 (2015).
- [17] J. yoon Choi, S. Hild, J. Zeiher, P. Schauß, A. Rubio-Abadal, T. Yefsah, V. Khemani, D. A. Huse, I. Bloch, and C. Gross, Science 352, 1547 (2016), https://www.science.org/doi/pdf/10.1126/science.aaf8834.

- [18] J. Smith, A. Lee, P. Richerme, B. Neyenhuis, P. W. Hess, P. Hauke, M. Heyl, D. A. Huse, and C. Monroe, Nature Physics 12, 907 (2016).
- [19] P. Bordia, H. Lüschen, U. Schneider, M. Knap, and I. Bloch, Nature Physics 13, 460 (2017).
- [20] A. Lukin, M. Rispoli, R. Schittko, M. E. Tai, A. M. Kaufman, S. Choi, V. Khemani, J. Léonard, and M. Greiner, Science 364, 256 (2019).
- [21] A. Rubio-Abadal, J.-y. Choi, J. Zeiher, S. Hollerith, J. Rui, I. Bloch, and C. Gross, Phys. Rev. X 9, 041014 (2019).
- [22] V. Oganesyan and D. A. Huse, Phys. Rev. B 75, 155111 (2007).
- [23] M. Žnidarič, T. c. v. Prosen, and P. Prelovšek, Phys. Rev. B 77, 064426 (2008).
- [24] A. Pal and D. A. Huse, Phys. Rev. B 82, 174411 (2010).
- [25] B. Bauer and C. Nayak, Journal of Statistical Mechanics: Theory and Experiment 2013, P09005 (2013).
- [26] A. D. Luca and A. Scardicchio, Europhysics Letters 101, 37003 (2013).
- [27] J. A. Kjäll, J. H. Bardarson, and F. Pollmann, Phys. Rev. Lett. 113, 107204 (2014).
- [28] D. J. Luitz, N. Laflorencie, and F. Alet, Phys. Rev. B 91, 081103 (2015).
- [29] C. Artiaco, F. Balducci, M. Heyl, A. Russomanno, and A. Scardicchio, Phys. Rev. B 105, 184202 (2022).
- [30] C. Artiaco, C. Fleckenstein, D. Aceituno Chávez, T. K. Kvorning, and J. H. Bardarson, PRX Quantum 5, 020352 (2024)
- [31] Y. Bar Lev, G. Cohen, and D. R. Reichman, Phys. Rev. Lett. 114, 100601 (2015).
- [32] F. Iemini, A. Russomanno, D. Rossini, A. Scardicchio, and R. Fazio, Phys. Rev. B 94, 214206 (2016).
- [33] E. V. Doggen, I. V. Gornyi, A. D. Mirlin, and D. G.

- Polyakov, Annals of Physics **435**, 168437 (2021), special Issue on Localisation 2020.
- [34] M. Serbyn, Z. Papić, and D. A. Abanin, Phys. Rev. Lett. 111, 127201 (2013).
- [35] D. A. Huse, R. Nandkishore, and V. Oganesyan, Phys. Rev. B 90, 174202 (2014).
- [36] J. Z. Imbrie, V. Ros, and A. Scardicchio, Annalen der Physik 529, 1600278 (2017).
- [37] G. D. Chiara, S. Montangero, P. Calabrese, and R. Fazio, Journal of Statistical Mechanics: Theory and Experiment 2006, P03001 (2006).
- [38] J. Eisert, M. Cramer, and M. B. Plenio, Rev. Mod. Phys. 82, 277 (2010).
- [39] J. H. Bardarson, F. Pollmann, and J. E. Moore, Phys. Rev. Lett. 109, 017202 (2012).
- [40] M. Serbyn, Z. Papić, and D. A. Abanin, Phys. Rev. Lett. 110, 260601 (2013).
- [41] D. Roy, R. Singh, and R. Moessner, Physical Review B 92, 10.1103/physrevb.92.180205 (2015).
- [42] F. Alet and N. Laflorencie, Comptes Rendus Physique 19, 498 (2018).
- [43] D. A. Abanin, E. Altman, I. Bloch, and M. Serbyn, Rev. Mod. Phys. 91, 021001 (2019).
- [44] P. Sierant, M. Lewenstein, A. Scardicchio, L. Vidmar, and J. Zakrzewski, arXiv e-prints 10.48550/arXiv.2403.07111 (2024).
- [45] W. De Roeck and F. m. c. Huveneers, Phys. Rev. B 95, 155129 (2017).
- [46] S. Gopalakrishnan and D. A. Huse, Phys. Rev. B 99, 134305 (2019).
- [47] K. Agarwal, E. Altman, E. Demler, S. Gopalakrishnan, D. A. Huse, and M. Knap, Annalen der Physik 529, 1600326 (2017).
- [48] I.-D. Potirniche, S. Banerjee, and E. Altman, Phys. Rev. B 99, 205149 (2019).
- [49] T. Szoldra, P. Sierant, M. Lewenstein, and J. Zakrzewski, Phys. Rev. B 109, 134202 (2024).
- [50] J. Léonard, S. Kim, M. Rispoli, A. Lukin, R. Schittko, J. Kwan, E. Demler, D. Sels, and M. Greiner, Nature Physics 19, 481 (2023).
- [51] H. P. Lüschen, P. Bordia, S. S. Hodgman, M. Schreiber, S. Sarkar, A. J. Daley, M. H. Fischer, E. Altman, I. Bloch, and U. Schneider, Phys. Rev. X 7, 011034 (2017).
- [52] D. J. Luitz, F. m. c. Huveneers, and W. De Roeck, Phys. Rev. Lett. 119, 150602 (2017).
- [53] L. Colmenarez, D. J. Luitz, and W. De Roeck, Phys. Rev. B 109, L081117 (2024).
- [54] J. C. Peacock and D. Sels, Phys. Rev. B 108, L020201 (2023).
- [55] D. Sels, Phys. Rev. B **106**, L020202 (2022).
- [56] Y.-T. Tu, D. Vu, and S. Das Sarma, Phys. Rev. B 107, 014203 (2023).
- [57] A. Morningstar, L. Colmenarez, V. Khemani, D. J. Luitz, and D. A. Huse, Phys. Rev. B 105, 174205 (2022).
- [58] Unrelated with the problem of the thermal inclusion, many works have studied the effect on MBL of a bath connected to the whole system [86–89].
- [59] S. Gopalakrishnan, M. Müller, V. Khemani, M. Knap, E. Demler, and D. A. Huse, Phys. Rev. B 92, 104202 (2015).
- [60] P. J. D. Crowley and A. Chandran, SciPost Phys. 12,

- 201 (2022).
- [61] H. Ha, A. Morningstar, and D. A. Huse, Phys. Rev. Lett. 130, 250405 (2023).
- [62] J. Colbois, F. Alet, N. Laflorencie, arXiv e-prints 10.48550/arXiv.2403.09608 (2024).
- [63] E. Levi, M. Heyl, I. Lesanovsky, and J. P. Garrahan, Phys. Rev. Lett. 116, 237203 (2016).
- [64] X. Cao, A. Tilloy, and A. De Luca, SciPost Phys. 7, 24 (2019).
- [65] P. Sierant and J. Zakrzewski, Phys. Rev. B 105, 224203 (2022).
- [66] L. Colmenarez, P. A. McClarty, M. Haque, and D. J. Luitz, SciPost Phys. 7, 064 (2019).
- [67] P. Sierant and J. Zakrzewski, Phys. Rev. B 99, 104205 (2019).
- [68] T. Chanda, P. Sierant, and J. Zakrzewski, Phys. Rev. B 101, 035148 (2020).
- [69] J. Šuntajs, J. Bonča, T. c. v. Prosen, and L. Vidmar, Phys. Rev. E 102, 062144 (2020).
- [70] M. Serbyn, A. A. Michailidis, D. A. Abanin, and Z. Papić, Phys. Rev. Lett. 117, 160601 (2016).
- [71] P. Sierant, M. Lewenstein, and J. Zakrzewski, Phys. Rev. Lett. 125, 156601 (2020).
- [72] E. V. H. Doggen, F. Schindler, K. S. Tikhonov, A. D. Mirlin, T. Neupert, D. G. Polyakov, and I. V. Gornyi, Phys. Rev. B 98, 174202 (2018).
- [73] E. Lieb, T. Schultz, and D. Mattis, Annals of Physics 16, 407 (1961).
- [74] R. Sidje, ACM Trans. Math. Softw. 24, 130 (1998).
- [75] P. Bordia, H. P. Lüschen, S. S. Hodgman, M. Schreiber, I. Bloch, and U. Schneider, Phys. Rev. Lett. 116, 140401 (2016).
- [76] D. J. Luitz, N. Laflorencie, and F. Alet, Phys. Rev. B 93, 060201 (2016).
- [77] For the smaller values of L, where relaxation times are shorter, we can use larger threshold, and get clearer exponential increases with W than the ones shown in Fig. 3(a).
- [78] J. T. Edwards and D. J. Thouless, Journal of Physics C: Solid State Physics 5, 807 (1972).
- [79] D. Thouless, Physics Reports 13, 93 (1974).
- [80] J. Šuntajs, J. Bonča, T. c. v. Prosen, and L. Vidmar, Phys. Rev. E 102, 062144 (2020).
- [81] P. Sierant, D. Delande, and J. Zakrzewski, Phys. Rev. Lett. 124, 186601 (2020).
- [82] G. De Tomasi, S. Bera, J. H. Bardarson, and F. Poll-mann, Phys. Rev. Lett. 118, 016804 (2017).
- [83] D. N. Page, Phys. Rev. Lett. 71, 1291 (1993).
- [84] Y. Bar Lev, G. Cohen, and D. R. Reichman, Phys. Rev. Lett. 114, 100601 (2015).
- [85] K. Slagle, Z. Bi, Y.-Z. You, and C. Xu, Phys. Rev. B 95, 165136 (2017).
- [86] M. H. Fischer, M. Maksymenko, and E. Altman, Phys. Rev. Lett. 116, 160401 (2016).
- [87] E. Levi, M. Heyl, I. Lesanovsky, and J. P. Garrahan, Phys. Rev. Lett. 116, 237203 (2016).
- [88] B. Everest, I. Lesanovsky, J. P. Garrahan, and E. Levi, Phys. Rev. B 95, 024310 (2017).
- [89] M. V. Medvedyeva, T. c. v. Prosen, and M. Žnidarič, Phys. Rev. B 93, 094205 (2016)